JOURNAL OF MATERIALS SCIENCE 33 (1998) 3555–3566

Single-crystal growth and characterization of Cu_2O and CuO

TAKAYUKI ITO*, HIROYUKI YAMAGUCHI*, KATSUYA OKABE‡, TAIZO MASUMI*§
*Department of Electronic Engineering, Gunma University, 1-5-1 Tenjin-cho, Kiryu, Gunma 376-8515, Japan
‡Gunma Prefectural College of Health Science, 323-1 Kamioki-cho, Maebashi, Gunma 371-0052, Japan
§Natural Research Institute for Metals, 1-2-1 Sengen, Tsukuba, Ibaraki 305-0047, Japan

We have prepared a large number of crystals of cuprous oxide (Cu_2O) by various procedures. Photoluminescence spectra of these crystals were studied to examine the concentration of defects, especially copper vacancy V_{Cu} to seek favourable conditions for growing Cu_2O crystal. High-quality single crystals of Cu_2O were prepared by the floating-zone melting method in air. Several synthetic crystals (specimens FA, FZ and GZ) and also a natural crystal were studied by X-ray analysis, inductively coupled plasma spectroscopy analysis, optical absorption, photoluminescence, photoconductivity and cyclotron resonance absorption, photoluminescence, photoconductivity and cyclotron resonance absorption to characterize their optical and electrical qualities. The best values of mobility and scattering time of photocarriers at $T = 4.2$ K are estimated to be $\mu_h \approx 1.8 \times 10^5$ cm^2 V^{-1} s^{-1} and $\tau_h \approx 60$ ps for positive holes, and $\mu_\bullet \approx 1.3 \times 10^5$ cm^2 V^{-1} s^{-1} and $\tau_\bullet \approx 70$ ps for electrons in Cu_2O. Further, we report preliminary experimental results on transport property of crystals also of cupric oxide (CuO) purified by the floating-zone melting method. © *1998 Kluwer Academic Publishers*

1. Introduction

Nature yields cuprous oxide (Cu_2O) and cupric oxide (CuO) as cuprite and tenorite, respectively. Cu_2O is a reddish p-type semiconductor of nature both ionic and covalent native with a direct forbidden band gap of 2.17 eV. A crystal of Cu_2O has a cubic structure (space group, $O_h^4 = pn3m$), having two molecules in the unit cell. This material is well known in the history of semiconductor physics and has been used as crystal rectifiers. Since a few of the hydrogen-like exciton series in absorption were observed in Cu_2O, its optical properties have been well investigated as a typical crystal for studying properties of excitons [1–7]. Recent reports on a possibility of the Bose condensation of excitons [8–12] and on the photoconductivity with anomalies at low temperatures [13–17] have attracted attention. Further investigations are being performed intensively and extensively.

For Cu_2O, however, it is known that the material usually includes considerable amounts of non-stoichiometry such as copper vacancies, V_{Cu}, and oxygen vacancies, V_O [18–27], but the correlation between these defects and electrical conductivity has not been understood in detail. Therefore, it is particularly important to make clear not only the methods of preparation of high-quality Cu_2O and the basic properties of electrical conductivity, etc., but also correlation between the former and the latter. In this paper, we report experimental results of a series of studies on the favourable conditions of annealing temperature, time for growing polycrystals, and vertical transfer and rotation rates in the floating-zone melting technique for growing single crystals. We have examined such conditions by estimating the concentration of lattice defects in photoluminescence spectra. Further, for three kinds of crystal prepared under these conditions and additionally for single crystals naturally grown in Zaire in Africa, we have investigated their physical properties by means of X-ray analysis, inductively coupled plasma (ICP) spectroscopy analysis, optical absorption, photoluminescence, photoconductivity and cyclotron resonance absorption in order to evaluate the quality of crystals from many aspects. As a result, we recognize that single crystals prepared by the floating-zone melting method in air (specimens FZ) are of the best quality not only from a view point of the concentration of defects but also from that of transport properties. Values of mobility and scattering time of photocarriers for specimen FZ were estimated to be about 1.8×10^5cm^2 V^{-1} s^{-1} and 60 ps in holes, and about 1.3×10^5cm^2 V^{-1} s^{-1} and 70 ps in electrons at $T = 4.2$ K.

CuO is a black semiconductor with a monoclinic structure (space group, $C2/c$) and is reported to have

a direct band gap of charge-transfer type with a value of 1.4 eV [28]. Although the material of CuO is a typical and common semiconductor, we still have poorer knowledge about this material than one expects. With the progress of studies on the high-T_C copper oxides in recent years, however, CuO has attracted attention as one of the simplest and most fundamental host materials. This is because of its antiferromagnetic spin ordering at low temperatures [29], in Cu^{2+} state [30], in CuO_2 planes [28], and its energy band gap of the charge-transfer type [28]. Recently, it has been indicated that CuO has strong electron correlation effects on the basis of the results of the energy band-structure calculations different from these obtained by photoelectron spectroscopies [28]. Thus, CuO has been observed with keener interest than ever. Nevertheless, there have been only a few reports available on the electrical conductivity, except in the vicinity of room temperature. In those papers, it is reported that CuO is a p-type semiconductor and its activation energy changes in the vicinity of the Néel temperature [31]. Because of difficulties in conductivity measurement owing to its high impedance, no detailed report is available on the electrical conductivity of CuO at lower temperatures. The thermoelectric effect indicates that the hole effective mass, m^*/m_0, is about 7.9 and this property suggests a small polaron [31], but this has not been confirmed directly by a cyclotron resonance experiment. To clarify this situation, we have refined CuO crystals by the floating-zone melting method and investigated the electrical conductivity of CuO especially down to $T = 4.2$ K by using a fast-pulse technique with blocking electrodes. We have also studied magnetoresistance and Hall effects by using pulsed photoconductivity measurements. It has been found that the value of mobility of photocreated holes in the prepared CuO crystal was estimated to be about 1.1×10^4 cm^2 V^{-1} s^{-1}. This suggests that the photocarriers in CuO are mobile in a wide energy band.

2. Preparation of specimens

2.1. Synthetic crystals of Cu_2O (specimens FA, FZ and GZ)

There have already been several reports on the methods of preparation of Cu_2O crystals, e.g., methods involving oxidization of copper [32, 33], melting growth [34, 35], floating zone [36–39] and hydrothermal growth [40]. We prepared polycrystals (specimens FA) by heating copper metal in air, and single crystals by the floating-zone melting method in air (specimens FZ) and under a low oxygen pressure (specimen GZ). Crystal growth by the floating-zone melting method was carried out by using the image furnace supplied by the NEC type SC-35HS with a halogen lamp as an energy source. The Cu–Cu_2O–CuO phase diagram reported by Schmidt-Whitly *et al.* [38] and displayed in Fig. 1, is basically referred to. In this section, we describe the methods of preparation of the artificial polycrystals FA, and the single crystals FZ and GZ refined by three different conditions.

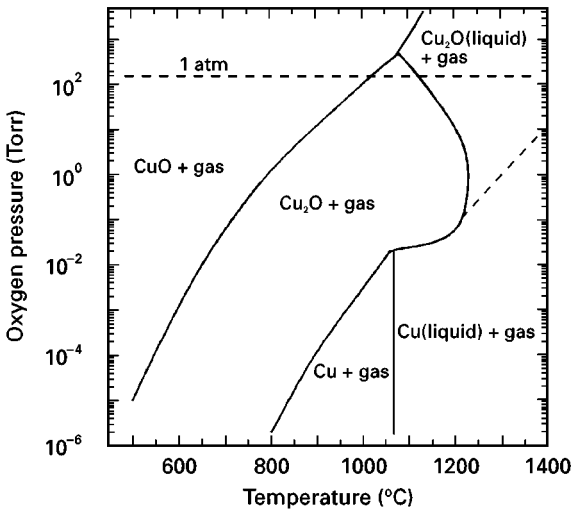

Figure 1 Phase diagram of the copper–oxygen system for pressure versus temperature. (After Schmidt-Whitley *et al.* [38]).

2.1.1. Polycrystals (furnace-annealed crystals FA)

We prepared polycrystalline bulk Cu_2O crystals as the first step for preparation of single crystals. As displayed in Fig. 1, Cu_2O crystals can be obtained easily by heating copper metal at high temperatures between 1020 and 1120 °C in air. The starting material was high-purity (99.999%) copper metal supplied by the High Purity Chemetals Co. Ltd, Saitama, Japan, in the form of rods with a radius of 5 mm and a length of 100 mm. The rod was washed with acetone and etched with dilute HNO_3. For use in a vertical furnace, the Cu rod was suspended by a platinum wire with a radius of 0.3 mm with a small hole drilled at one end of the specimen. We obtained rods of polycrystalline Cu_2O by oxidizing completely at an annealing temperature, T_a, of 1050 °C for an annealing time, t_a, of 100 h and by cooling at about 160 °C h^{-1}, all in air. The area of grains in the Cu_2O specimen FA obtained by oxidizing at high temperatures was at most 1 mm × 1 mm.

2.1.2. Single crystals (floating-zone crystals FZ and GZ)

We have prepared high-quality single crystals by the floating-zone melting method in air. As "feed rods", specimens FA were prepared by heating at 1050 °C for 100 h and cooling naturally in air as described in Section 2.1.1. Rods of the polycrystalline Cu_2O obtained were set up in the imaging furnace. Incidentally, not only the polycrystalline Cu_2O specimen FA but also raw copper metal was set up in the imaging furnace. In the case of the latter, however, a melting zone could not be formed with the standard power of the imaging furnace. We consider that the temperature of the specimens does not rise sufficiently because the high thermal conductivity of copper metal causes a heavy loss of heat from the focused part. The polycrystalline specimens FA or the resulting single crystals FZ were used as "seed rods". We prepared specimens FZ under a vertical transfer rate of 3.5 mm h^{-1} and a melting-zone rotation rate 7 rev min^{-1}

opposite directions for the "seed rod" and the "feed rod", all in air.

Further, we prepared specimens GZ by the floating-zone melting method under an argon pressure, P(Ar), of 2 atm with 3% oxygen.

A photograph of the cross-sections of specimens FA and FZ is displayed in Fig. 2a as a typical example of the specimens obtained.

Details of the conditions determined for growing specimens FA, FZ and GZ will be discussed in Section 5.

2.2. Natural single crystals of Cu_2O

We prepared single crystals naturally grown in Zaire in Africa as reference materials for artificially grown crystals. As displayed in Fig. 2b, a blue-and-green material, probably olivine ($(Mg, Fe)_2SiO_4$) and/or malachite ($Cu_2CO_3(OH)_2$) , adheres to the specimen. Considerable impurities may be included in this Cu_2O phase. In our study here, after removing the impurity phases judged by their colours, the crystals were cut, polished and etched; these specimens will be called natural specimens hereafter.

2.3. Synthetic crystals of CuO

Techniques of flux growth [41], sublimation [42] and chemical vapour transport [43–45] have been adopted as methods of crystal growth of CuO. In order to suppress the inclusion of impurities as small as possible, we tried to grow single crystals of CuO by the floating zone melting method. Reagent-grade powders of CuO were placed into a drain tube, pressed at a static water pressure of 600 kgf cm^{-2} and sintered at 900 °C for 3 days in air. Rods of sintered CuO were set up in the imaging furnace. The molten zone travelled at a vertical transfer rate of 5 mm h^{-1}, and rotation rates of 7 rev min^{-1} were employed in opposite directions for "seed rod" and "feed rod" under an oxygen pressure, $P(O_2)$, of 2 atm. At the present stage of the trial production, we obtained bulk crystals of radius about 5 mm and length about 50 mm. A photograph of a cross-section of the CuO crystal obtained is displayed in Fig. 2c. From the observation of crystal surface by scanning electron microscopy (SEM) shown in Fig. 2d, the maximum area of the crystal grains obtained was confirmed to be of the order of 1 mm × 1 mm

3. Experimental procedures

Specimens of Cu_2O were cut out to be about 5 mm × 5 mm × 0.03–0.05 mm in size for optical absorption measurements, about 5 mm × 3 mm × 0.5 mm in size for photoluminescence and photoconductivity measurements and about 1 mm × 1 mm × 0.5 mm in

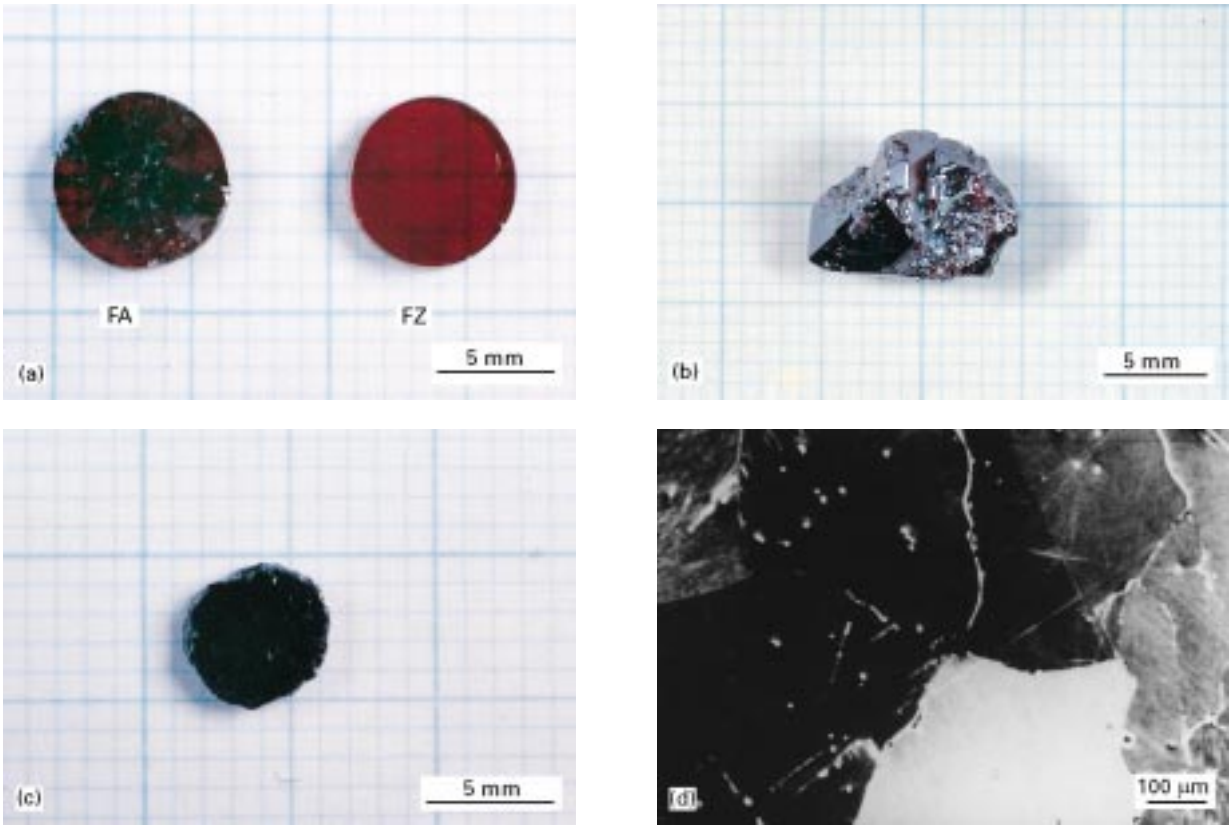

Figure 2 (a) A photograph of a typical Cu_2O specimen FA obtained by oxidization for 100 h at 1050 °C and a Cu_2O specimen FZ obtained by the floating-zone melting method with a vertical transfer rate of 3.5 mm h^{-1} and a rotation rate of 7 rev min^{-1} in opposite directions for the seed rod and feed rod in air. The starting material is high purity copper metal 99.999%. The divisions are 1 mm. (b) A typical example of single-crystal Cu_2O naturally grown in Zaire in Africa (before elimination of impurities). The divisions are 1 mm. (c) A typical photograph of a CuO specimen obtained by the floating-zone melting method with a vertical transfer rate of 5 mm h^{-1} and a rotation rate of 7 rev min^{-1} in opposite directions for the seed rod and feed rod under an oxygen pressure, $P(O_2)$ of 2 atm. The divisions are 1 mm. (d) A scanning electron micrograph of a CuO specimen obtained by the floating-zone melting method with a vertical transfer rate of 5 mm h^{-1} and a rotation rate of 7 rev min^{-1} in opposite directions for the seed rod and feed rod under an oxygen pressure, $P(O)_2$, of 2 atm. The scale bar is 100 μm. Note that blue section lines can be recognized through CuO specimen.

size for cyclotron resonance measurements. They were polished mechanically using Al_2O_3 powders and etched chemically using 2% KCN solution. Each specimen was cut from the same vicinity in the same rods.

An X-ray analysis was carried out using a Rigaku diffractometer type RAD-2C with a copper target at a tube voltage of 40 kV and a tube current of 30 mA for powder and a Rigaku diffractometer type PSPC-MDG 2000 with a chromium target at a tube voltage of 40 kV and a tube current of 150 mA for crystals.

An ICP spectroscopy analysis was carried out using a Japanese Jarrell–Ash Corporation type ICAP 575. Qualitative and quantitative analyses were performed with 1 g of crushed specimen in 100 ml of HCl(1 + 1).

Optical absorption measurements were carried out using a Fourier transform spectrometer of Bruker type IFS-113V with a resolution of $\Delta\nu = 1\,cm^{-1}$.

In photoluminescence measurements, a continuous-wave Ar-ion laser was used at a wavelength λ_{ex} of 514.5 nm with a power of 5 mW as a light source. The modulation frequency of the laser beam was 275 Hz. A Spex 1672 double monochromator (whose reciprocal dispersion was $2\,nm\,mm^{-1}$ with gratings of $1200\,lines\,mm^{-1}$ installed) was used for $\lambda = 600$–1100 nm with appropriate photomultipliers. The photosignals were amplified and phase-sensitively detected by a lock-in amplifier.

Because of the high impedance of Cu_2O and CuO at low temperatures, measurements of transport properties were performed mainly by a transient method for photoconductivity with blocking electrodes and by microwave cyclotron resonance at 35 GHz. Owing to the low density of carriers and the resultant high-impedance, nature, it is difficult to measure the electrical conductivity of most insulating semiconductors at low temperatures by the conventional four-probe method. The only method which avoids these measurement difficulties and gives highly credible information is the pulsed photoconductivity technique with blocking electrodes. This technique has been described in detail in [16, 46, 47].

The photoconductive signals, Q, detected are proportional to the density of the photocarriers and the transfer distance of photocarriers. The drift mobility, μ_d obtained by a time-of-flight method, the magnetoresistance mobility, μ_M, obtained by the magnetoresistance effect and the Hall mobility, μ_H, obtained from the Hall effect can be calculated using photoconductivity measurements. The magnetoresistance and Hall mobility are estimated from $\mu_M = (c/H)\,[Q_x(0)/Q_x(H) - 1]^{1/2}$ and $\mu_H = (c/H)Q_y(H)/Q_x(H)$, respectively, where H is the applied magnetic field. Because the macroscopic drift mobility is influenced by shallow traps especially at low temperatures, we measured the magnetoresistance and the Hall mobility in this investigation, which are almost equal to the microscopic mobility determined only by the energy band structure and the scattering mechanism. Information on the effective mass and scattering time of photocarriers can be obtained directly from cyclotron resonance absorption.

As a light source for photoexcitation, a yttrium-aluminium-garnet-laser-pumped dye laser and a Ti–sapphire laser with a duration of 10 ns, a repetition rate of 13 Hz and a power of $10\,mJ\,pulse^{-1}$ were used at an excitation light wavelengths, λ_{ex}, of 735 nm and 850 nm respectively. In the case of cyclotron resonance experiments, a xenon flash lamp (output energy about $30\,\mu J\,pulse^{-1}$; pulse width, about 0.5 μs) was used at 13 Hz. Light for photoexcitation illuminated the crystal surface via an optical fibre and/or a quartz rod. Photosignals were amplified and detected by a Boxcar integrator.

4. Results

4.1. Cu_2O (Specimens FA, FZ and GZ and the natural specimens)

4.1.1. Quality of specimens

Fig. 3a displays X-ray powder diffraction patterns of four Cu_2O crystals. The lattice constants, a, of each specimen are 4.259 Å for specimen FA, 4.261 Å for specimen FZ, 4.271 Å for specimen GZ and 4.262 Å for the natural specimen.

Although specimen FA is an impure dark-red colour, specimens FZ and GZ are clear red. The impure dark-red colour of specimen FA may indicate the extrinsic inclusion of portions of CuO, because a few peaks of impurity phases corresponding to CuO have been recognized in part of specimen FA by X-ray analysis as displayed in Fig. 3b. Further, copper deposits or pores and voids are also considered as candidates which cause the black colour in the Cu_2O crystal specimen FA. In specimens FZ and GZ and the natural specimen, peaks due to CuO are not detectable by X-ray analysis.

Fig. 3c displays the X-ray diffraction pattern of the cross-section of specimen FZ. This clearly indicates that the specimen is a single crystal and the cross-section is the (100) plane. That is, the growth of specimens prepared by the floating-zone melting method is oriented along the [100] direction.

In order to study unfavourable inclusions of impurities besides CuO, we analysed each specimen by electron probe microanalysis (EPMA). As a result, a few peaks due to different kinds of atom such as Si and Al were detected only in the natural specimen. Further, we carried out ICP spectroscopy analysis of a natural Cu_2O specimen which has a total amount of impurities such as Si, Fe, Mg and Al of up to 1080 ppm as summarized in Table I. These results may be ascribed to extrinsic inclusions of ingredients such as olivine ($(Mg, Fe)_2SiO_4$) in cuprous oxide ore.

TABLE I Identification and amount of impurities in natural Cu_2O by ICP spectroscopy analysis.

Element	Na	Mg	Al	Si	P	K	Ca	Mn	Fe	Ni	Zn	Ag	Pb
Amount of inclusions (ppm)	30	40	30	620	0	0	90	0	270	0	0	0	0

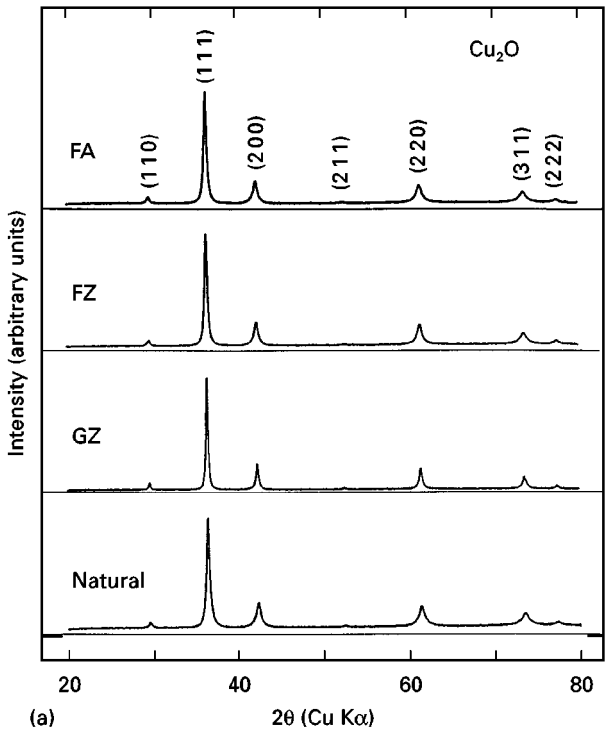

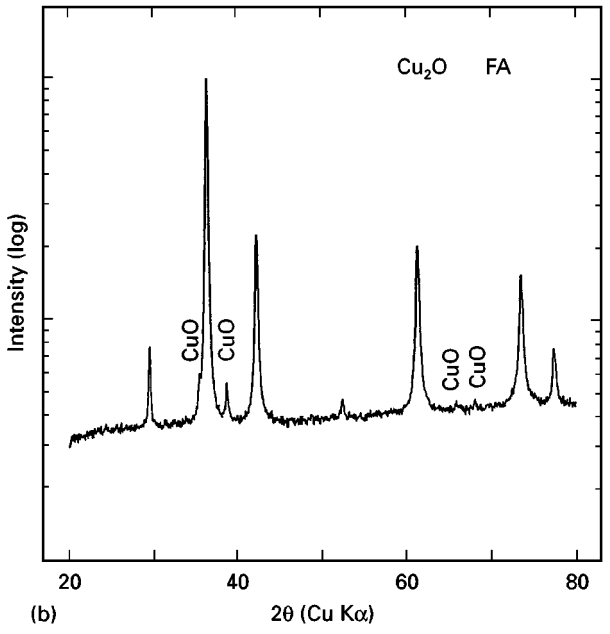

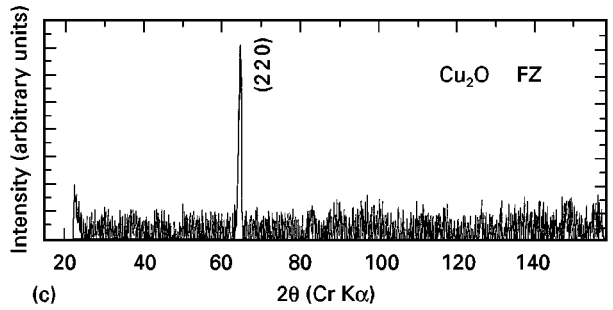

Figure 3 (a) X-ray powder diffraction patterns of four Cu_2O single crystals. The natural Cu_2O specimen was measured after impurity phases as judged from colours were removed. (b) Enlarged X-ray powder diffraction pattern of polycrystalline specimen FA Cu_2O obtained by oxidization for 100 h at 950 °C in air. (c) X-ray diffraction pattern of a single-crystal Cu_2O specimen FZ obtained by floating zone melting method.

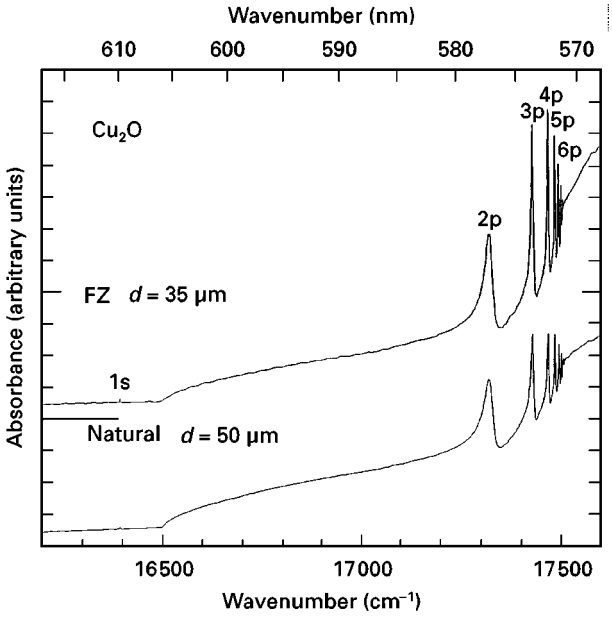

Figure 4 Optical absorption spectra of Cu_2O at $T = 5.2$ K. A series of exciton absorptions up to $n = 10$ are observed.

4.1.2. Optical and electrical properties

Fig. 4 displays typical traces of the optical absorption spectra of a Cu_2O specimen FZ and natural specimen at $T = 5.2$ K. Independent of the purity and quality of the specimens, a series of exciton absorption up to $n = 10$ are observed [48]. Since we discussed the optical absorption spectra in detail elsewhere, we confine ourselves here to a brief explanation in Section 5.

Fig. 5a displays photoluminescence spectra in near-infrared region of four Cu_2O crystals photoexcited by an Ar-ion laser at $T = 4.2$ K. One can readily recognize significant differences between their luminescence spectra. The V_{Cu} luminescence band observed at $\lambda \approx 910$ nm has been attributed to copper vacancies. The V_O bands observed at $\lambda \approx 720$ and 820 nm have been attributed to oxygen vacancies; in particular the former is ascribed to doubly ionized oxygen vacancies, $V_{O^{2+}}$ and the latter to singly ionized vacancies, V_{O^+} [18, 21, 27].

In determining the method of preparation described in Section 2, we studied various conditions from the view point not only of reducing impurities but also controlling the concentration of vacancies. Here, we performed experiments of evaluation by using the fact that the photoluminescence spectra of Cu_2O are dependent on the conditions of preparation of specimens which affect the stoichiometric proportions. An object here is to evaluate specimens from the viewpoint of the concentration of copper vacancies which are the main defects in Cu_2O.

In order to seek favourable conditions for growing specimens FA, we prepared several specimens at annealing temperatures, T_a, of 950 –1100 °C and annealing times, t_a, of 70–300 h. Fig. 5b displays the relation between the annealing temperature, T_a, and the luminescence intensity of the V_{Cu} band at $T = 77$ K for an annealing time, t_a of 100 h. Fig. 5c displays the relation between the annealing time, t_a, and the luminescence intensity of the V_{Cu} band at $T = 77$ K

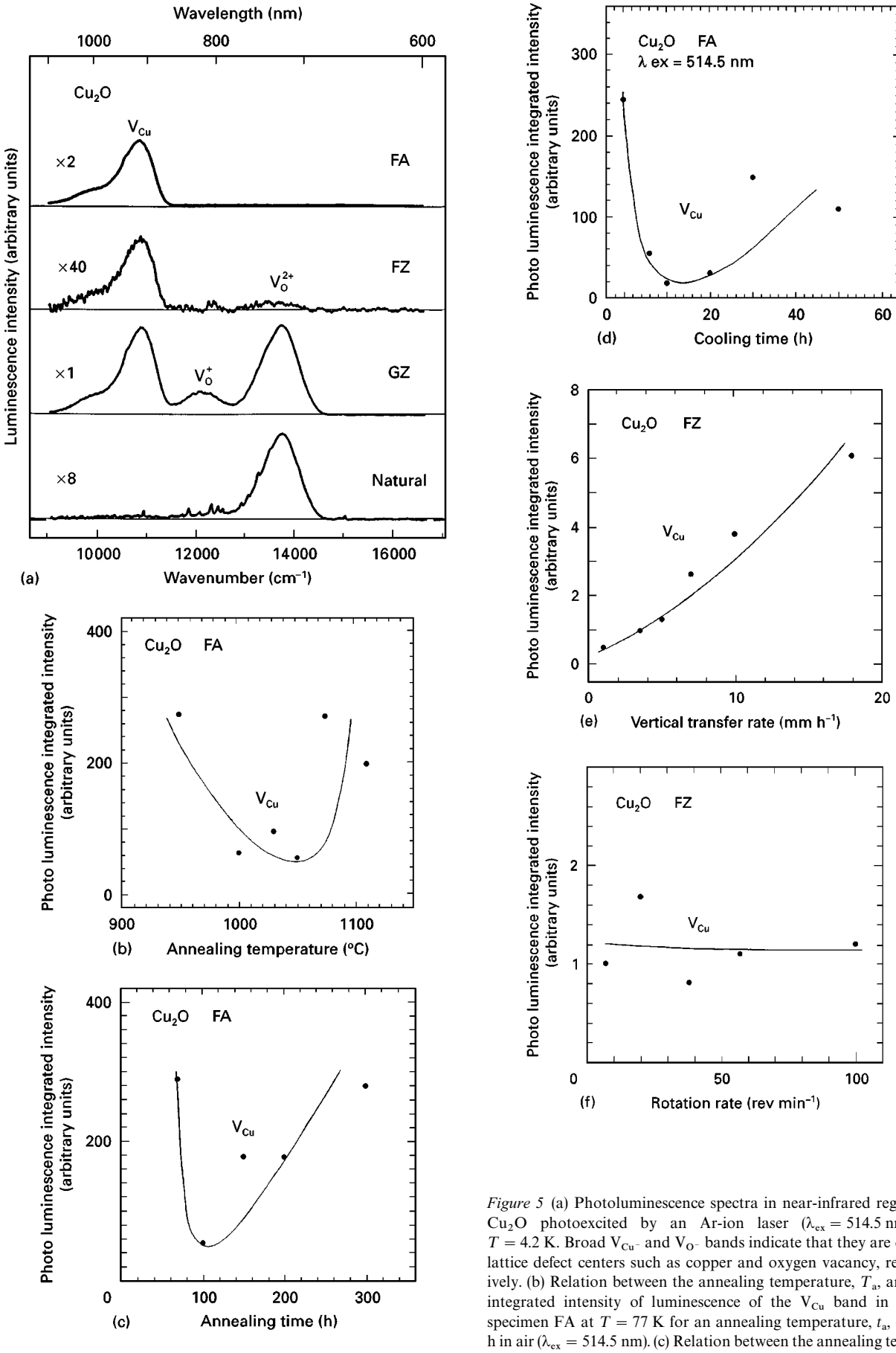

Figure 5 (a) Photoluminescence spectra in near-infrared region of Cu_2O photoexcited by an Ar-ion laser ($\lambda_{ex} = 514.5$ nm) at $T = 4.2$ K. Broad V_{Cu}- and V_{O}- bands indicate that they are due to lattice defect centers such as copper and oxygen vacancy, respectively. (b) Relation between the annealing temperature, T_a, and the integrated intensity of luminescence of the V_{Cu} band in Cu_2O specimen FA at $T = 77$ K for an annealing temperature, t_a, of 100 h in air ($\lambda_{ex} = 514.5$ nm). (c) Relation between the annealing temperature, t_a, and the integrated intensity of luminescence of the V_{Cu} band in Cu_2O specimen FA at $T = 77$ K for an annealing temperature, T_a, of 1050 °C in air ($\lambda_{ex} = 514.5$ nm). (d) Relation between the cooling time and integrated intensity of luminescence of the V_{Cu} band in Cu_2O specimen FA at $T = 77$ K for an annealing temperature, T_a, of 1050 °C and annealing time, t_a, of 100 h in air ($\lambda_{ex} = 514.5$ nm). (e) Relation between the vertical transfer rate and the integrated intensity of luminescence of the V_{Cu} band in Cu_2O specimen FZ at $T = 77$ K for a rotation rate of 7 rev min^{-1} in opposite directions for the "seed rod" and the "feed rod" in air ($\lambda_{ex} = 514.5$ nm). (f) Relation between the rotation rate and the integrated intensity of luminescence of the V_{Cu} band in Cu_2O specimen FZ at $T = 77$ K for a vertical transfer rate of 3.5 mm h^{-1} in air ($\lambda_{ex} = 514.5$ nm).

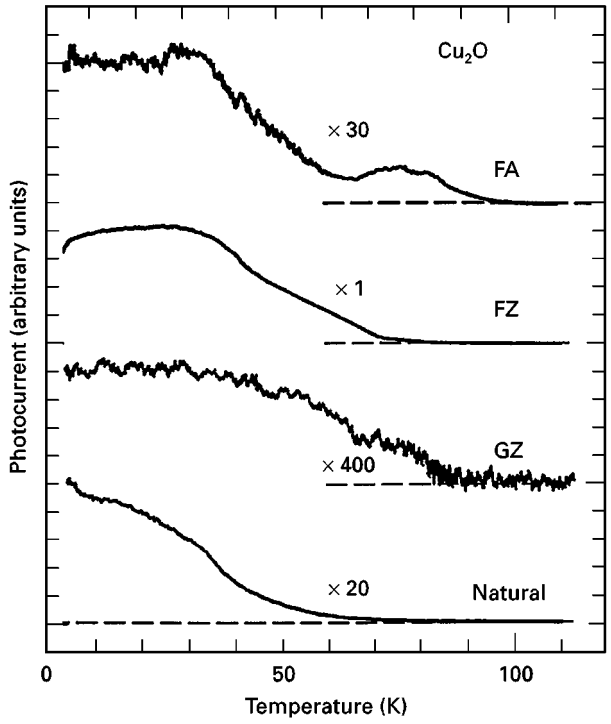

Figure 6 Temperature dependence of pulsed photoconductivity of four Cu_2O crystals at $\lambda_{ex} = 735$ nm and $E = 0.1\,kV\,cm^{-1}$.

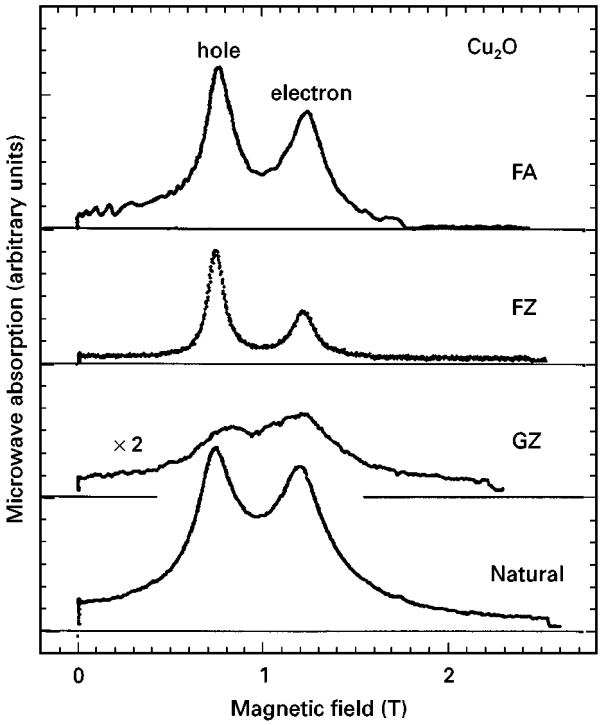

Figure 7 Microwave absorption in cyclotron resonance of photocarriers in Cu_2O for xenon flash-lamp excitation at $f = 35$ GHz and $T = 4.2$ K.

for an annealing temperature, T_a, of 1050 °C. Fig. 5d displays the relation between the cooling time and the luminescence intensity of the V_{Cu} band at $T = 77$ K for $T_a = 1050$ °C and $t_a = 100$ h.

In order to study favourable conditions for growing specimens FZ, we prepared several specimens with vertical transfer rates of 1–18 mm h^{-1} and the rotation rates of the melting zone of 7–100 rev min^{-1} in the opposite direction for the "seed rod" and the "feed rod", all in air. Fig. 5e displays the relation between the vertical transfer rates and the luminescence intensity of the V_{Cu} band at $T = 77$ K. Fig. 5f displays the relation between the rotation rates and the luminescence intensity of the V_{Cu} band at $T = 77$ K.

We made supplementary experiments of pulsed photoconductivity and microwave cyclotron resonance absorption due to photocarriers for four Cu_2O crystals to evaluate their quality from the viewpoint of transport properties at low temperatures. In the present experiments, measurement conditions such as the intensity of photoexcitation and applied electric field are fixed for all specimens.

Fig. 6 displays the temperature dependence of photoconductivity of four Cu_2O crystals at $\lambda_{ex} = 735$ nm and $E = 0.1\,kV\,cm^{-1}$. In this λ_{ex} region, the valance electrons can be excited only to localized levels such as vacancies located in the energy gap; thus only free positive holes are mobile. Although the absolute value of photoconductivity varies considerably among different specimens, the unique behaviour of the photoconductivity of Cu_2O with anomalies increasing with decreasing temperature remains similar and universal over these specimens.

Fig. 7 illustrates traces of the microwave cyclotron resonance absorption due to photocarriers in four Cu_2O crystals at xenon flash excitation, $f = 35$ GHz and $T = 4.2$ K. One can observe two resonance lines both for holes and for electrons. The line width is narrower in specimens FZ and is broader in specimens GZ and natural specimens.

4.2. CuO

The lattice constants of CuO are determined to be $a = 4.713$ Å, $b = 3.420$ Å, $c = 5.135$ Å and $\beta = 99.58°$ from the X-ray diffractions pattern in Fig. 8. For comparison, X-ray diffraction patterns for the reagents of Cu_2O and CuO are also illustrated.

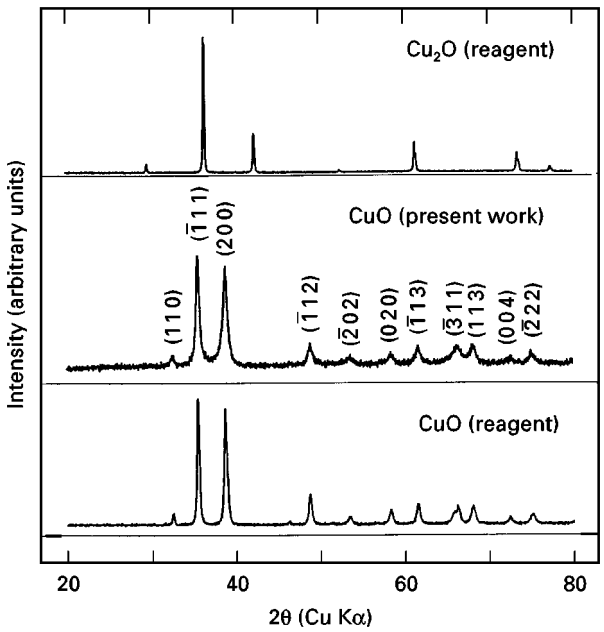

Figure 8 X-ray powder diffraction pattern of CuO crystals obtained by the floating-zone melting method under $P(O_2) = 2$ atm. For a comparison, those of the reagent-grade Cu_2O and CuO specimens are also indicated.

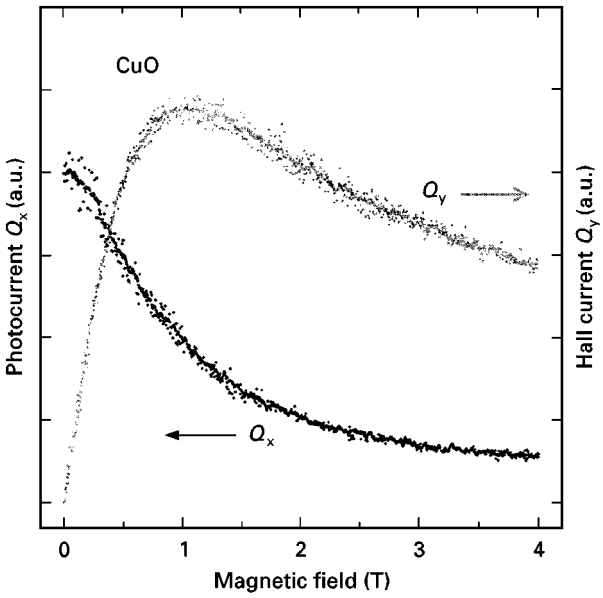

Figure 9 Magnetic field, H_z, dependence of photocurrent, Q_x, and Hall current, Q_y, due to positive holes in CuO at $\lambda_{ex} = 850$ nm, $E_x = 0.1\,\mathrm{kV\,cm^{-1}}$ and $T = 4.2$ K. Note that Q_y in a transient photoconductivity represents the Hall Current and not the Hall Voltage.

Fig. 9 displays the magnetic field dependence of the photoconductivity, $Q(H)$, of CuO at $T = 4.2$ K. Q_x represents the photocurrent signal in the direction of the electric field, and Q_y represents the Hall current signal in the direction perpendicular to both the electric and the magnetic fields. The wavelength of photoexcitation is $\lambda_{ex} = 850$ nm, where only positive holes can be excited. Q_y in transient photoconductivity represents the Hall current and not the Hall voltage, but, we can treat the Hall current here as equivalent to the Hall voltage to estimate value of the Hall mobility, μ_H, of photocarriers. From these results of the positive magnetoresistance effect and the transient Hall effect, both the magnetoresistance mobility, μ_M, and the Hall mobility, μ_H, of photocreated positive holes are estimated to be about $1.1 \times 10^4\,\mathrm{cm^2\,V^{-1}s^{-1}}$.

5. Discussion

5.1. Cu_2O (specimens FA, FZ and GZ and natural specimens)

5.1.1. Conditions of crystal growth

Here, we first discuss favourable conditions for growing Cu_2O. In the case of crystal growth by oxidation of copper, the luminescence intensity of the V_{Cu} band has a minimum in the vicinity of $T_a = 1050\,^\circ$C and increases not only at lower annealing temperatures but also at higher annealing temperatures as displayed in Fig. 5b. The phenomenon at lower annealing temperatures may be ascribed to the conversion from CuO with imperfections to Cu_2O because the specimens obtained have a black colour. On the other hand, the higher annealing temperature increased the grain size, but annealing at high temperatures above 1075 °C caused the introduction of imperfections into the specimens. Since the prepared rod had bent slightly by annealing at high temperatures above 1075 °C, we consider that the luminescence intensity of the V_{Cu} band increases because of evaporation of some of the copper atoms in the raw rod as the first step of melting causes a decrease in the volume and the distortion of crystals. Consequently, we consider that the most favourable annealing temperature lies in the vicinity of 1050 °C. In this case, the luminescence intensity of the V_{Cu} band has a minimum in the vicinity of the annealing time, t_a, of 100 h, as displayed in Fig. 5c. It takes at least 40 h to oxidize the rod of copper metal completely. If the annealing time is shorter than 40 h, a raw copper block remains in the centre of specimen. From these simple considerations, we expect the quality of specimens to be better for longer annealing times because the time of growth of Cu_2O crystals increases. Certainly, up to an annealing time, t_a, of 100 h, the luminescence intensity of the V_{Cu} band decreases with increasing annealing time, t_a. However, a further increase on the annealing time causes an increase in the concentration of copper vacancies. Therefore, this suggests that factors exist which result in deterioration in the quality of specimens on excessively increasing the annealing time, t_a, e.g., the removal of copper atoms from the crystal surface. As a result, high-quality specimens can be obtained by annealing for a long time at the boundary of the CuO–Cu_2O phases or $T_a = 1020$–$1025\,^\circ$C. When a time of 6–20 h to cool was employed from 1050 °C to room temperature (cooling rates, 50–160 °C h^{-1}) as displayed in Fig. 5d, the luminescence intensity of the V_{Cu} band indicates a minimum value. We consider that rapid cooling causes distortion of the specimens, and very slow cooling causes instability of the Cu_2O phase with the growth of the CuO phase under stable conditions for the CuO phase.

In the case of the crystal growth by the floating-zone melting method, the concentration of copper vacancies increases monotonically with increase in the vertical transfer rate of the molten zone or the rate of crystal growth, as displayed in Fig. 5e. Thus, one may expect that a crystal of higher quality is obtained with slower rates of crystal growth, but the slower vertical transfer rate requires a technique that maintains a molten zone. As displayed in Fig. 5f, no particular correlation can be recognized within the limits of measurements in the relation between the rotation rate of the molten zone and the concentration of vacancies in the specimens. It is preferable to set the vertical transfer rate at $3.5\,\mathrm{mm\,h^{-1}}$ and the rotation rate at $7\,\mathrm{rev\,min^{-1}}$ in opposite directions for the "seed rod" and the "feed rod", so that the most stable molten zone can be sustained.

Since the V_{Cu} band is dominant over the V_O bands in specimens FA and FZ, we have tried to grow specimens GZ under a lower oxygen pressure. Only in argon gas flowing free from oxygen gas, did we find copper deposits on the prepared specimens because of the reducing effect. Thus, we tried to grow specimens under an argon pressure, P(Ar), of 2 atm with 3% oxygen in order to prevent copper deposits due to the reducing effect, but, the luminescence intensity for the specimens obtained to further increased not only for the V_O bands but also for the V_{Cu} bands. Consequently, we consider that one can control the

TABLE II Favourable conditions for Cu_2O specimen preparation by the oxidation of copper metal.

Annealing temperature	1050 °C
Annealing time	100 h
Cooling rate	50–160 °C h^{-1}

TABLE III Favourable conditions for the floating-zone melting method of Cu_2O.

Vertical transfer rate	3.5 mm h^{-1}
Rotation rate	7 rev min^{-1}
Atmosphere	Air

concentrations of copper and oxygen vacancies by regulation of the partial pressures of oxygen but cannot simultaneously reduce them. It is recognized that the concentration of copper vacancies decreases considerably or the quality of crystals is improved by use of the floating-zone melting method in air as displayed in Fig. 5a. Finally, favourable conditions for growing Cu_2O are summarized in Tables II and III.

5.1.2. Characterization of specimens

As displayed in Fig. 4, independent of the purity and the quality of specimens, a series of exciton absorption up to $n = 10$ are observed in the Yellow series. Little difference is observed between the optical absorption spectra in the region of exciton absorption for Cu_2O specimens FZ and for natural specimens. However, slight differences in linewidth and relative oscillator strength of each state of the exciton series can be seen. Although the natural specimens have a total amount of impurities up to 1080 ppm as reported in Table I, no significant difference exists between the optical absorption spectra of these specimens.

On the contrary, in the luminescence spectra in Fig. 5a, we observe significant differences for the specimens. It shows a set of luminescence spectra of the V_{Cu} band at $\lambda \approx 910$ nm with the $V_{O^{2+}}$ band at $\lambda \approx 720$ nm for specimens FZ. The latter is only a eighth of the former. Only the luminescence of the V_{Cu} band is observed for specimen FA. The intensity of the V_{Cu} band for specimen FA is about 18 times larger than that for specimen FZ, whereas the luminescence of $V_{O^{2+}}$ band is not observed for specimen FA. This may be caused by difference in the amount of oxygen during growth. Oxygen penetrates relatively easily into rods of FA. For specimen FZ, however, since oxygen is received only from surface of the specimen, the amount of oxygen in the crystals is less than that for specimen FA. All the V_{Cu} band and V_O bands appear prominently for specimen GZ. The intensity of the $V_{O^{2+}}$ band for specimen GZ is about 300 times larger and the intensities of the V_{Cu} band about 40 times larger than for specimen FZ. Further, the V_{O^+} band at around 820 nm also appears for specimen GZ. On the other hand, for the natural specimen, the luminescence intensity of the V_{Cu} band is smaller than that for specimen FZ, but the $V_{O^{2+}}$ band appears prominently and its intensity is about 38 times larger than that for specimen FZ. The V_{O^+} band appears as a shoulder for the natural specimen. This may reflect that crystals had grown better under a low-oxygen concentration atmosphere deep inside the earth. Further details of the photoluminescence of Cu_2O have been reported in [48].

In order to evaluate the quality of Cu_2O crystals from transport properties at low temperatures, we have carried out supplemental measurements of the pulsed photoconductivity, $Q(T, \lambda)$, and the cyclotron resonance absorption of Cu_2O at 35 GHz. From simple considerations, one may suppose that copper and oxygen vacancies reduce the lifetime of photocarriers and the density of carriers and consequently, the magnitude of photoconductivity. The photoconductivity of the Cu_2O specimen FZ including the lowest concentration of defects has the largest absolute value, and that of specimen GZ including the highest concentration of defects has the smallest absolute value. The absolute value of the photoconductivity of specimen GZ is smaller than that of the natural specimen including the most impurities.

Since specimens FA, FZ and GZ were made of identical starting materials, it is considered that there is no difference between the concentrations of impurities in these but there is between the concentrations of copper and oxygen vacancies. If we assume that the luminescence intensity due to vacancies is proportional to the concentration of defects, the absolute value of photoconductivity, $Q(T, \lambda)$, may be influenced mainly by the concentration of vacancies and not by the concentration of metallic impurities. However, the onset temperatures of photoconductivity are more or less similar for various specimens. This is an enigma. Previously, it was reported that Cu_2O material usually includes copper vacancies at concentrations as high as 10^{18}–10^{19} cm^{-3} and oxygen vacancies at concentrations as high as 10^{17}–10^{18} cm^{-3} by the usual methods of preparation [18, 22–24]. Since the purity of copper metal as a material is 99.999%, the concentration of impurities included in specimens FA, FZ and GZ is of the order of 10^{18} cm^{-3}, which is a similar level to those of copper and oxygen vacancies. On the other hand, the total concentration of impurities in natural Cu_2O is enormous, as indicated in Table I. Thus, one realizes that the capture cross-sections of defect levels due to impurities, etc., for photocarriers must be extremely small. This strange situation due to curious states is supported also by the temperature dependence of the photoconductivity, $Q(T, \lambda)$. Since the energy levels due to copper and oxygen vacancies lie 0.55 eV above that of the valance band and 0.38 eV below that of the conduction band, respectively [24], these should act as a deep level at temperatures below 100 K. Shallow levels due to impurities or strains usually capture photocarriers. As a result, the number of photocarriers decreases exponentially with decreasing temperature. However, the photoconductivity, $Q(T, \lambda)$, of Cu_2O exhibits little decrease; rather it increases with decreasing temperature, especially below 100 K. Even in natural Cu_2O, although the concentrations of impurities are

TABLE IV Characterization of Cu_2O and CuO specimens by four different methods, i.e., photoluminescence, photoconductivity, mobility and time of scattering of photocarriers at $T = 4.2$ K, where the photoluminescence intensity is indicated as ratio to the intensity of the $V_{O^{2+}}$ band in specimen GZ, the magnitude of photoconductivity is indicated as the ratio to the photoconductivity specimen FZ at $T = 4.2$ K, and the physical parameters in CuO are also indicated as reference data.

Specimen	Purity (%)	Photoluminescence intensity (%)			Photoconductivity at 4.2 K (%)	Mobility ($cm^2\ V^{-1}\ s^{-1}$)		Scattering time (ps)	
		V_{Cu}	$V_{O^{2+}}$	V_{O^+}		μ_h	μ_e	τ_h	τ_e
FA	99.999	41	—	—	5.0	115 000	88 000	40	50
FZ	99.999	2.3	0.3	—	100	179 000	127 000	60	70
GZ	99.999	95	100	11	0.3	62 000	40 000	23	22
Natural	1080 ppm (impurity)	0.2	12	0.4	7.7	84 000	58 000	29	32
CuO	Reagent grade	—	—	—		11 000	—	4	—

enormously high as recognized in Section 4.1.1, its photoconductivity also indicates a similar increase with decreasing temperature as displayed in Fig. 6. Incidentally, even in specimens Fa and FZ made of copper metal 99.9% purity, their photoconductivities indicate a similar tendency in the temperature dependence. These results suggest that there are no shallow levels of about 10 me V due to impurities or strains or for unknown reasons, the capture of photocarriers into shallow levels become ineffective at low temperatures in Cu_2O. The difference between the absolute values of photoconductivity for various specimens may be caused by imperfections such as vacancies in the Cu_2O crystals themselves. Because of not only the behaviour of $Q(T, \lambda)$, which enhances stability with decreasing temperature, but also the emergence of a series of exciton absorptions up to $n = 10$ independent of the quality of specimens, we consider that a correlation may emerge between photocarriers at low temperatures and that a many-body effect beyond the one-electron energy band scheme in conventional semiconductor physics occurs in Cu_2O. This physical interpretation has been described in detail elsewhere [13–17] (see in particular [16]).

In the case when the effective mass of carrier is isotropic and uniform over its energy surface, the microwave absorption is represented by

$$P = \tfrac{1}{2}\sigma_0 E_\omega^2 \frac{1 + (\omega_c^2 + \omega^2)\tau^2}{[1 + (\omega_c^2 - \omega^2)\tau^2]^2 + 4\omega^2\tau^2}, \quad (1)$$

where E_ω, σ_o, ω_0 and τ denote the amplitude of microwave field, the DC conductivity, the cyclotron frequency and the scattering time, respectively. By fitting each line of the cyclotron resonance absorption in Fig. 7 to Equation 1, the scattering times, τ_h, of holes, are estimated to be 40 ps, 60 ps, 23 ps and 29 ps, and the scattering times, τ_{-e}, of electrons, to be 50 ps, 70 ps, 22 ps and 32 ps for specimen FA, specimen FZ, specimen GZ and the natural specimen, respectively. Consequently, the mobilities, μ_k, of positive holes, are calculated to be 115 000 $cm^2\ V^{-1}\ s^{-1}$, 179 000 $cm^2\ V^{-1}\ s^{-1}$, 62 000 $cm^2\ V^{-1}\ s^{-1}$, 84 000 $cm^2\ V^{-1}\ s^{-1}$ and the mobilities, μ_e, of electrons to be 88 000 $cm^2\ V^{-1}\ s^{-1}$, 127 000 $cm^2\ V^{-1}\ s^{-1}$, 40 000 $cm^2\ V^{-1}\ s^{-1}$, 58 000 $cm^2\ V^{-1}\ s^{-1}$ for specimen FA, specimen FZ, specimen GZ and the natural specimen respectively. Characterization of four Cu_2O crystals are summarized in Table IV. The parameters τ_h and τ_e depend on various kinds of defect, mostly vacancies but also including impurities. Thus, we consider that, with the subsidiary roles of impurities, it is mainly the existence of vacancies which influence the values of mobility, scattering time and lifetime of phtocarriers in Cu_2O at low temperatures.

5.2. CuO

There is a possibility that Cu_2O may remain as an impurity phase in CuO crystals obtained by the floating-zone melting method. No impurity phases can be found in CuO here in the X-ray powder diffraction pattern in Fig. 8. Further, also from anomalies in the magnetic susceptibility at the Néel temperatures, $T_{N1} = 230$ K and $T_{N2} = 213$ K, and the emergence of peaks due to antiferromagnetic ordering in Raman spectra below the Néel temperature, we have confirmed the crystals obtained here to be genuine CuO. Basic properties such as optical absorption in CuO will be reported elsewhere [49, 50].

Only a few reports are available on the electrical conductivity of CuO. Koffyberg and Benko [31] reported that the effective mass and mobility of positive holes are about $7.9m_0$ and 0.1 $cm^2\ V^{-1}\ s^{-1}$, respectively, for Li-doped CuO at $T = 300$ K [31]. They considered that the behaviour of carriers in CuO can be expressed using the small polaron model. On the other hand, our experimental results in Fig. 9 indicate that the mobility of photocreated positive holes is comparatively large, about 1.1×10^4 $cm^2\ V^{-1}\ s^{-1}$ at $T = 4.2$ K.

Further, in CuO, we have succeeded in observing also microwave cyclotron resonance absorption at 35 GHz. The scattering time of photocarriers in CuO is short, $\tau_h \leqslant 4$ ps at $T = 4.2$ K. These physical properties are summarized in Table IV. Although the present situation is still at the preliminary stage, the results obtained so far are consistent with the results of the magnetoresistance and transient Hall effect. Namely, these results suggest that photocarriers in CuO are mobile in a wide energy band. We shall investigate directly the effective mass of photocarriers by cyclotron resonance absorption and report them elsewhere [50] in the future.

The materials of Cu_2O and CuO usually include impurities and non-stoichiometry. Nevertheless, the mobility of photocarriers in these specimens at low temperatures is much larger than in silver halides of super-high purity [47]. Since the transport properties in Cu_2O and CuO have not been studied in detail, its true mechanism requires further investigation in future. Here, we are concerned mainly with reporting the crystal growth and characterization of Cu_2O and CuO.

6. Summary

We have prepared a large number of bulk crystals of Cu_2O under various conditions and characterized the crystals by X-ray analysis, optical absorption, photoluminescence, pulsed photoconductivity and cyclotron resonance absorption. We have paid special attention not only to reducing the concentration of impurities but also to controlling the concentration of defects and imperfections such as vacancies during crystal growth. By performing mainly X-ray analysis and photoluminescence measurements, we established the favourable conditions for growing Cu_2O crystals: annealing temperature, $T_a = 1050\,^{\circ}C$; annealing time, $t_a = 100\,h$; cooling rates, 50–160 $^{\circ}C\,h^{-1}$; vertical transfer rate, $3.5\,mm\,h^{-1}$; rotation rate, $7\,rev\,min^{-1}$. Single-crystal specimens FZ grown by the floating zone technique in air are of the highest quality and exhibit the following values of mobility and scattering times of photocarriers at $T = 4.2\,K$; $\mu_h \approx 1.8 \times 10^5\,cm^2\,V^{-1}\,s^{-1}$ and $\tau_h \approx 60$ ps for holes; and $\mu_\bullet \approx 1.3 \times 10^5\,cm^2\,V^{-1}\,s^{-1}$ and $\tau_\bullet \approx 70$ ps for electrons. All these results suggest that the capture of photocarriers due to impurities is ineffective at low temperature below 100 K in Cu_2O.

Further, in these studies, we have performed also a set of preliminary experiments on the magnetoresistance and Hall effect of CuO crystals purified by the floating-zone melting technique. As a result the main photocarriers in CuO at $T = 4.2\,K$ are confirmed to be positive holes. The mobility is $\mu_h \approx 1.1 \times 10^4\,cm^2\,V^{-1}\,s^{-1}$. This result suggests that photocarriers in CuO are mobile in the wide energy band in contrast with the results reported by Koffyberg and Benko.

We emphasize that the role of imperfections in specimens may be more important than the role of impurities in order to clarify the optical and electrical properties of Cu_2O and CuO.

Acknowledgements

The authors would like to express their sincere thanks to the faculty members of the Department of Electronic Engineering, Gunma University. We thank Dr S. Mimotogi for his cooperation in the preliminary stage of optical experiments, Messrs K Saito and M. Shijo for providing us with some data on optical absorption and microwave cyclotron resonance, and Mr T. Ozawa (Gunma Prefectural Industrial Technology Research Laboratory) for his cooperation in the ICP spectroscopy analysis. This work was supported by Grants-in-Aid especially for the Specially Promoted Research and for Scientific Research (A) in its respective stages, both from the Ministry of Education, Science and Culture, Japan.

References

1. M. HAYASHI and K. KATSUKI, *J. Phys. Soc. Jpn* **5** (1950) 380.
2. E. F. GROSS, *Nuovo Cimento Suppl.* **3** (1956) 672.
3. S. NIKITINE, in "Optical properties of solids" (Plenum, New York, 1969) Section 9.
4. K. SHINDO, T. GOTO and T. ANZAI, *J. Phys. Soc. Jpn* **36** (1974) 753.
5. T. ITOH and S. NARITA, *ibid.* **39** (1975) 132.
6. *Idem.*, *ibid.* **39** (1975) 140.
7. V. I. AGEKYAN, *Phys. Status Solidi (a)* **43** (1977) 11.
8. D. SNOKE, J. P. WOLFE and A. MYSYROWICZ, *Phys. Rev. Lett.* **64** (1990) 2543.
9. D. W. SNOKE and J. P. WOLFE, *Phys. Rev. B* **39** (1989) 4030.
10. D. W. SNOKE, J. P. WOLFE and A. MYSYROWICZ, *Phys. Rev. Lett.* **64** (1990) 2543.
11. *Idem.*, *Phys. Rev. B* **41** (1990) 11 171.
12. J. L. LIN and J. P. WOLFE, *Phys. Rev. Lett.* **23** (1993) 1222.
13. H. SHIMADA and T. MASUMI, *J. Phys. Soc. Jpn* **58** (1989) 1717.
14. T. MASUMI. *ibid.* **60** (1991) 3625.
15. T. MASUMI and H. SHIMADA, *ibid.* **60** (1991) 3633.
16. T. MASUMI, *Phase Transitions* **51** (1994) 127.
17. H. AMEKURA and T. MASUMI, *J. Phys. Soc. Jpn* **64** (1995) 2684.
18. J. BLOEM, *Philips Res. Rep.* **13** (1958) 167.
19. I. S. GORBAN' *et al.*, *Sov. Phys.—Solid State* **3** (1962) 1559.
20. F. M. BERKOVSKII and YU. G. SHRETER, *Sov. Phys.—Semicond.* **2** (1968) 631.
21. N. A. TOLSTOI and V. A. BONCH-BRUEVICH, *Sov. Phys.—Solid State* **13** (1971) 1135.
22. B. PREVOT, C. CARABATOS and M. SIESKIND, *Phys. Status Solidi (a)* **10** (1972) 455.
23. M. ZOUAGHI, *ibid.* **11** (1972) 219.
24. M. ZOUAGHI, B. PREVOT and C. CARABATOS, *ibid.* **11** (1972) 449.
25. K. T. CHEE, T. KEOWSIM and F. L. WEICHMAN, *Can. J. Phys.* **57** (1979) 988.
26. S. V. GASTEV, A. A. KAPLYANSKII and N. S. SOKOLOV, *Solid State Commun.* **42** (1982) 389.
27. C. K. TEH and F. L. WEICHMAN, *Can. J. Phys.* **61** (1983) 1423.
28. J. GHIJSEN, L. H. TJENG, J. VAN ELP, H. ESKES, J. WESTERINK, G. A. SAWATZKY and M. T. CZYZYK, *Phys. Rev. B* **38** (1988) 11 322.
29. A. JUNOD, D. ECKERT, G. TRISCONE, J. MULLER and W. REICHARDT, *J. Phys.: Condens. Matter* **1** (1989) 8021.
30. W. Y. CHING, Y. N. XU and K. W. WONG, *Phys. Rev. B* **40** (1989) 7684.
31. F. P. KOFFYBERG and F. A. BENKO, *J. Appl. Phys.* **53** (1982) 1173.
32. R.S. TOTH, R. KILKSON and D. TRIVICH, *ibid.* **31** (1960) 1117.
33. Y. EBISUZAKI, *ibid.* **32** (1961) 2027.
34. T. NAKANO, K. OHTANI, A. KINOSHITA and T. OKUDA, *Jpn. J. Appl. Phys.* **5** (1964) 124.
35. A. KINOSHITA and T.NAKANO, *ibid.* **5** (1966) 1121.
36. D. TRIVICH and G.P. POLLACK, *J. Electrochem. Soc.* **117** (1970) 344.
37. W. S. BROWER Jr and H. S. PARKER, *J. Cryst. Growth* **8** (1971) 227.
38. R. D. SCHMIDT-WHITLEY, M. MARTINEZ-CLEMENTE and A. REVCOLEVSCHI, *ibid.* **23** (1974) 113.
39. J. L. LOISON, M. ROBINO and C. SCHWAB, *ibid.* **50** (1980) 816.
40. A. KINOSHITA and T. NAKANO, *Jpn J. Appl. Phys.* **6** (1967) 656.

41. B. M. WANKLYN and B. J. GARRARD, *J. Mater. Sci. Lett.* **2** (1983) 285.
42. Th. W. J. PIETERS and J. NEDERMEYER, *J. Cryst. Growth* **15** (1972) 299.
43. N. YAMAMOTO, Y. BANDO and T. TAKADA, *Jpn J. Appl. Phys.* **12** (1973) 1115.
44. W. DEISTO, B. T. COLLINS, R. KERSHAW, K. DWIGHT and A. WOLD, *Mater. Res. Bull.* **24** (1989) 1005.
45. E. C. MILLIKEN and J. F. CORDARO, *J. Mater. Res.* **5** (1990) 53.
46. M. UETA, H. KANZAKI, K. KOBAYASHI, Y. TOYOZAWA and E. HANAMURA, in "Excitonic processes in solids" (Springer, Berlin, 1986) Section 8.
47. T. MASUMI, in "Quasi-particle physics in condensed matter" (Baifukan, Tokyo, 1986) (in Japanese).
48. T. ITO and T. MASUMI, *J. Phys. Soc. Jpn* **66** (1997) 2185.
49. T. MASUMI, H. YAMAGUCHI, T. ITO and H. SHIMOYAMA, *ibid.* **67** (1998) 67.
50. H. YAMAGUCHI, T. ITO and T. MASUMI, *ibid.* **67** (1998) 1102 and in preparation.

Received 5 August 1997
and accepted 2 April 1998.